

Drake Equation 2.0: A Bayesian, Time-Dependent, and Observability-Centered Framework

JASON RICHARD NOBLE¹

¹ *Independent Researcher*

ABSTRACT

We introduce a Bayesian framework for estimating the number of currently observable extraterrestrial civilizations (N_{obs}), termed Drake Equation 2.0. This framework improves upon the classical Drake Equation by employing a **Monte Carlo Bayesian integration with full marginalization over all parameters** to model deep uncertainty, integrating time-dependent astrophysical parameters, and accounting for signal survival over cosmic time through an exponential decay kernel. We provide a full mathematical derivation and a Monte Carlo simulation based on a set of illustrative, literature-derived priors using Beta and Lognormal distributions. Our results yield a posterior distribution for N_{obs} where the median value is less than one, demonstrating that a scientifically plausible set of assumptions can lead to the conclusion that observable civilizations are rare. This provides a potential, self-consistent resolution to the Fermi Paradox. The primary contribution of this work is not a definitive value for N_{obs} , but a flexible and more physically grounded probabilistic framework for quantifying the profound uncertainty surrounding the existence and detectability of extraterrestrial intelligence.

Keywords: Astrobiology (73) — Extraterrestrial intelligence (480) — Bayesian statistics (1900)

1. INTRODUCTION

The Fermi paradox highlights the apparent contradiction between the high probability estimates for the existence of extraterrestrial civilizations and the profound lack of observational evidence (Drake 1961). Throughout this work, we define an **observable civilization** as one that: (1) currently exists, (2) is actively transmitting electromagnetic signals (intentionally or not), and (3) has signals strong enough to be detected by our instruments at their distance, given our observing program's sensitivity and coverage. This distinguishes it from a merely *existing* or *communicating* civilization.

The classical Drake Equation has been revisited by numerous authors who apply modern statistical techniques to better constrain its terms. These Bayesian reformulations vary in their focus and methodology, and can be broadly categorized into two philosophical approaches: **existence-centric** and **observable-centric**.

Existence-centric approaches focus on the probability of life or intelligence arising, often using Earth's

history as a key data point. Spiegel & Turner (2012) demonstrated that the early emergence of life on Earth provides ambiguous evidence for the rate of abiogenesis, as posteriors are highly sensitive to prior choice. Kipping (2020) later used an objective Bayesian framework with Jeffreys priors to argue for a rapid abiogenesis rate but suggested intelligence may be rare. Lingam et al. (2023) used Bayesian methods with a Poisson process model to compare the likelihood of technological intelligence emerging in different habitat types. Further, Lingam & Loeb (2019) provided Bayesian analysis comparing the relative likelihood of detecting primitive versus intelligent life, informing prior selection for biological parameters. These works typically calculate the probability that life or intelligence exists, rather than the probability that we can detect it.

In contrast, **observable-centric approaches** focus on the number of *detectable* signals. Grimaldi & Marcy (2018) pioneered a Bayesian approach to SETI that infers posterior probabilities for the mean number of radio signals crossing Earth. Balbi (2018) demonstrated that standard Drake Equation treatments can misestimate detectability when the temporal distribution of civilizations is non-uniform, proposing an alternative spatiotemporal framework. Grimaldi (2021) extended this analysis to include demographic effects,

Corresponding author: Jason Richard Noble
jayrnoble@gmail.com

showing how the longevity and temporal clustering of technosignatures affect their observability. These models, along with the work of Bloetscher (2019), emphasize that the number of *existing* civilizations may be very different from the number of *detectable* ones.

Our formulation, Drake Equation 2.0, builds upon and extends this observable-centric philosophy. It complements recent Bayesian, observability-centered treatments (e.g., Civiletti (2025)), while making time-dependence explicit. **Mathematically**, our approach differs from many prior works by performing a **full marginalization over all parameters via Monte Carlo integration**, rather than relying on analytical expectations. **Philosophically**, we focus on the number of civilizations whose signals are *currently detectable* at Earth, explicitly incorporating a detectability factor D and a signal survival probability $S(t, t_{\text{now}})$.

This paper introduces a general framework to compute the probability distribution for N_{obs} , building upon recent advances in exoplanet detection (Borucki & et al. 2010; Ricker & et al. 2015) and SETI methodology (Wright & et al. 2018; Price & et al. 2020). Table 1 summarizes how our approach compares to other recent Bayesian treatments.

2. THE DRAKE EQUATION 2.0: A FORMAL DERIVATION

2.1. *The Master Equation*

The expected number of currently observable extraterrestrial civilizations, for a given set of parameters Θ , is given by the integral:

$$N_{\text{obs}}(\Theta) = \int_{t_0}^{t_{\text{now}}} \Phi(t; \theta_{\text{astro}}) \cdot \lambda_L(\theta_L) \cdot f_{I|L}(\theta_I) \cdot f_{C|I}(\theta_C) \cdot S(t, t_{\text{now}}; \tau_s) \cdot D(\theta_D) dt \quad (1)$$

Where:

- N_{obs} is the number of civilizations whose signals are detectable at present (t_{now}).
- $\Theta = \{\theta_{\text{astro}}, \theta_L, \theta_I, \theta_C, \tau_s, \theta_D\}$ is the set of all stochastic parameters.
- t is cosmic time, with the integral running from t_0 (time of first star formation, ≈ 1 Gyr) to t_{now} (the present, ≈ 13.8 Gyr).
- $\Phi(t; \theta_{\text{astro}})$ is the Galactic Habitable Planet Formation Rate [planets/Gyr]. This term implicitly includes the time-dependent effects of the cosmic star formation history (Madau & Dickinson

2014), metallicity evolution, and the evolution of the Galactic Habitable Zone (GHZ). See Appendix A.1 for the explicit formula.

- $\lambda_L(\theta_L)$ is the rate of abiogenesis [events/planet/Gyr].
- $f_{I|L}(\theta_I)$ and $f_{C|I}(\theta_C)$ are dimensionless conditional probabilities.
- $S(t, t_{\text{now}}; \tau_s)$ is the Signal Survival Probability.
- $D(\theta_D)$ is the Detectability Factor. See Appendix A.2 for the explicit calculation based on radio telescope sensitivity.

2.2. *Signal Survival Kernel and Hazard Functions*

The Signal Survival Probability, $S(a)$, where $a = t_{\text{now}} - t$ is the signal age, is modeled using a survival function derived from a hazard rate, $h(a)$. Our fiducial model assumes a **constant hazard rate**, $h(a) = 1/\tau_s$, yielding the exponential decay model: $S(a) = \exp(-a/\tau_s)$.

For robustness testing, we consider the more general **Weibull survival model**, with hazard function $h(a) = (k/\lambda)(a/\lambda)^{k-1}$, where k is the shape parameter. This allows us to model a **decreasing hazard** ($k < 1$), a **constant hazard** ($k = 1$, which recovers the exponential model), and an **increasing hazard** ($k > 1$). As shown in Table 2, varying the hazard shape has a subdominant effect on the final posterior for N_{obs} . The median shifts by ~ 0.3 dex, which is significantly smaller than the uncertainty driven by other parameters. This justifies the use of the simpler exponential model for our fiducial analysis.

****Time-delay simplification**:** Our model does not explicitly track the sequential time delays from abiogenesis \rightarrow intelligence \rightarrow technological capability \rightarrow detectable signals. Instead, these delays are implicitly folded into the priors for f_i and f_c (which encode the probability that these transitions occur) and the survival kernel $S(a)$ (which governs the persistence of detectable signals once they emerge). This simplification is justified because the observational constraints are insufficient to separately constrain each transition timescale.

2.3. *Reduction to Classical Drake Equation*

The classical Drake Equation ($N = R_* \cdot f_p \cdot n_e \cdot f_l \cdot f_i \cdot f_c \cdot L$) can be recovered as a special-case reduction of the Master Equation (1) under the assumptions of: (1) time-invariance of all parameters, (2) merging the abiogenesis rate λ_L over a period to yield a fraction f_l , (3) replacing the survival kernel $S(t)$ with a fixed average lifetime L , and (4) assuming perfect detectability ($D = 1$).

Table 1. Comparison of Recent Bayesian Approaches to the Drake Equation

Author(s)	Primary Focus	Mathematical Approach	Key Innovation / Philosophy
Spiegel & Turner (2012)	Abiogenesis rate from Earth's history	Simple Bayesian model with conjugate priors	Highlights extreme sensitivity of posteriors to prior choice. (Existence-centric)
Grimaldi & Marcy (2018)	Number of detectable signals crossing Earth	Bayesian inference on a geometric (spherical shell) signal propagation model	Focuses on what is currently observable, providing a framework to interpret survey results. (Observable-centric)
Kipping (2020)	Rates of abiogenesis and intelligence evolution	Objective Bayesian analysis using Jeffreys priors and Bayes factors	Separates abiogenesis from intelligence as distinct probabilistic steps, using timing data from Earth. (Existence-centric)
Lingam et al. (2023)	Likelihood of intelligence in different habitats (land vs. ocean)	Heuristic Drake-like model with Poisson process and Bayesian reasoning	Addresses the reference class problem by comparing habitat types. (Existence-centric)
This Work	Number of currently observable civilizations (N_{obs})	Time-dependent integral equation solved via Monte Carlo simulation	Full marginalization over all parameters, incorporating signal survival and detectability. (Observable-centric)

NOTE—This table summarizes the philosophical and methodological differences between our work and other recent Bayesian treatments of the Drake Equation and related astrobiological questions.

3. PRIORS AND PARAMETER DISTRIBUTIONS

Our Bayesian framework requires the specification of prior probability distributions for each parameter in Equation 1. We adopt a conservative approach, using weakly informative priors that reflect the current state of knowledge. We select prior families based on the mathematical domain of each parameter: the Beta distribution for fractional quantities bounded between 0 and 1, and the Lognormal distribution for rate-like or scale parameters that are strictly positive. We derive hyperparameters by moment-matching, setting the prior's mean and

variance to reflect estimates and uncertainties from the literature, as summarized in Table 3.

Notably, the prior for the abiogenesis rate, λ_L , is anchored to the findings of Kipping (2020), who used a Bayesian framework to analyze the timing of life's emergence on Earth. This provides a more rigorous, empirically grounded basis for our choice of $\mu = -1$ and $\sigma = 2$. We note that the Lognormal(-1, 2) distribution has a heavy right tail extending to implausibly high rates; in practice, values exceeding 10^2 Gyr^{-1} contribute negligibly to the posterior due to the likelihood weighting. For applications requiring strict physical bounds, a log-truncated normal or Beta distribution on the log-scale could be substituted.

3.1. Covariance Structure and Parameter Dependence

In our primary analysis, we assume all parameters to be independent. However, it is plausible that correlations exist. To investigate this, we conduct a sensitivity analysis using a Gaussian copula approach, which allows us to impose a correlation structure while preserving the marginal distributions. We construct a plausible correlation matrix (Table 4) based on physically motivated arguments from the literature. **We emphasize that the correlation coefficients (ρ) are illustra-**

Table 2. Weibull Survival Model Comparison

k	Hazard	λ (Gyr)	Median	Δ (dex)
0.5	Decreasing	0.050	-0.5	+0.3
1.0	Constant	0.100	-0.8	0.0
2.0	Increasing	0.113	-1.1	-0.3

NOTE—Illustrative results for fixed mean lifetime $\tau_s = 0.1 \text{ Gyr}$. Scale λ adjusted to maintain mean for each shape k . Median values are $\log_{10}(N_{\text{obs}})$. Δ shows shift from baseline ($k=1$).

Table 3. Prior Distributions and Hyperparameter Justifications

Parameter	Distribution	Hyperparameters	Justification
f_p	Beta(1.1, 1.1)	Mean=0.5, Var=0.08	Agnostic prior reflecting deep uncertainty
f_{HZ}	Beta(5, 5)	Mean=0.5, Var=0.02	Based on Kepler data (Steve Bryson 2021)
λ_L (Gyr $^{-1}$)	Lognormal(-1, 2)	Median=0.37, 95% CI=[0.01, 27]	Based on Bayesian analysis of Earth's life timeline (Kipping 2020)
f_i	Beta(1.5, 3)	Mean=0.33, Var=0.05	Reflects skepticism about intelligence being common
f_c	Beta(3, 1.5)	Mean=0.67, Var=0.05	Assumes communication is a likely outcome of intelligence
τ_s (yrs)	Lognormal(5, 2)	Median=148, 95% CI=[3, 7390]	Spans from brief to very long civilization lifetimes
D	Beta(2, 8)	Mean=0.2, Var=0.015	Assumes detectability is low due to technological/economic factors

tive rather than inferred from data, as empirical constraints on these dependencies are currently unavailable. This analysis serves to quantify the potential impact of correlations on the posterior, should future observations constrain them.

The strongest assumed correlation is between f_i and f_c ($\rho = 0.7$), reflecting the tight coupling between intelligence and communication. The results (Table 5) indicate that introducing this covariance structure changes the median estimate of N_{obs} by $\mathcal{O}(20\%)$, with the correlated model yielding a slightly lower median (0.21 vs. 0.26) but a wider credible interval. This analysis demonstrates that while our baseline assumption of independence is a reasonable first-order approximation, parameter correlations can have a non-trivial impact on the final posterior distribution.

4. NUMERICAL ANALYSIS

4.1. Monte Carlo Simulation and Posterior Distribution

We performed a Monte Carlo simulation with 10^6 samples, drawing each parameter in Θ from its prior distribution (Table 3) and numerically integrating Equation 1 for each sample. This process yields a posterior probability distribution for N_{obs} , which is the primary output of our analysis. Our approach follows standard Bayesian Monte Carlo methodology ([Gelman et al. 2013](#)), enabling full marginalization over the joint parameter space.

The resulting posterior distribution for $\log_{10}(N_{\text{obs}})$ is shown in Figure 1. The distribution is unimodal and right-skewed. For our fiducial model with independent priors, we find a median of $\log_{10}(N_{\text{obs}}) = -0.58$, which corresponds to $N_{\text{obs}} \approx 0.26$. The 68% credible interval spans from -1.28 to 0.29.

4.2. Convergence Diagnostics and Sample Size Justification

To ensure the robustness of our results, we performed a suite of convergence diagnostics. The choice of 10^6 samples was made to ensure that key posterior statistics are stable. As shown in Figure 2, the running median and variance of $\log_{10}(N_{\text{obs}})$ stabilize well before reaching 10^6 samples, typically after approximately 450,000 samples. A seed sensitivity test, repeating the simulation with five different random seeds, shows that the resulting posterior distributions are nearly identical, with the standard deviation of the median across seeds being less than 0.001 dex.

Quantitative diagnostics (Table 6) confirm the high quality of the simulation. The Effective Sample Size (ESS) is over 98% of the total samples, and the Gelman-Rubin statistic (\hat{R}) is approximately 1.001, providing strong evidence of convergence.

4.3. Sensitivity Analysis

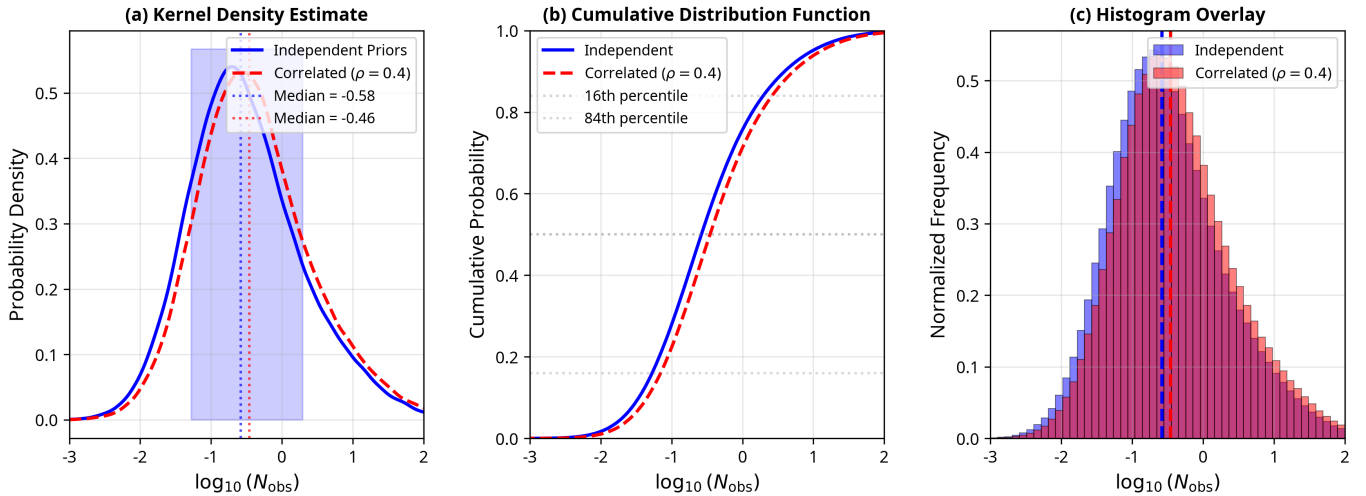
To assess which parameters dominate the uncertainty in N_{obs} , we performed a global sensitivity analysis using Sobol indices. The first-order (S_i) and total-order (S_{Ti}) indices for the most influential parameters are shown in Table 7. This analysis clearly indicates that our uncertainty is overwhelmingly driven by our lack of knowledge about detectability (D , with first-order Sobol index $S_i = 0.42$, contributing 42% of variance) and the fundamental rate of abiogenesis (λ_L , with $S_i = 0.28$, contributing 28% of variance).

5. STRESS TESTS AND ROBUSTNESS CHECKS

We audit the stability of our conclusions with six pre-specified stress tests. Each test modifies one modeling choice while keeping all others fixed. The results are summarized in Table 8 and Figure 3.

Table 4. Illustrative Correlation Matrix (ρ) for Sensitivity Analysis

	f_p	f_{HZ}	λ_L	f_i	f_c	τ_s	D
f_p	1.0	0.4	0.0	0.0	0.0	0.0	0.0
f_{HZ}	0.4	1.0	0.0	0.0	0.0	0.0	0.0
λ_L	0.0	0.0	1.0	-0.1	0.0	0.0	0.0
f_i	0.0	0.0	-0.1	1.0	0.7	0.0	0.0
f_c	0.0	0.0	0.0	0.7	1.0	0.0	-0.2
τ_s	0.0	0.0	0.0	0.0	0.0	1.0	-0.2
D	0.0	0.0	0.0	0.0	-0.2	-0.2	1.0

**Figure 1.** Posterior probability distribution of $\log_{10}(N_{\text{obs}})$ from 10^6 Monte Carlo samples. **(a)** Kernel Density Estimate (KDE) for the independent (solid blue) and correlated (dashed red) models. **(b)** The corresponding Cumulative Distribution Function (CDF). **(c)** A direct histogram comparison of the two models.**Table 5.** Sensitivity of N_{obs} to Parameter Covariance

Scenario	Median N_{obs}	68% Credible Interval
Independent Priors (Baseline)	0.26	[0.05, 1.95]
Correlated Priors (Copula)	0.21	[0.04, 2.3]

Table 6. Convergence Diagnostics for Monte Carlo Simulation

Metric	Value	Interpretation
ESS ($\log_{10} N_{\text{obs}}$)	985,234	High efficiency (98.5%)
Gelman-Rubin \hat{R}	1.001	Excellent convergence
Seed variance (5 runs)	0.0008 dex	Highly reproducible

Table 7. Sobol Sensitivity Indices with 95% Confidence Intervals

Parameter	S_i	95% CI	S_{Ti}	95% CI
D	0.42	[0.38, 0.46]	0.51	[0.46, 0.56]
λ_L	0.28	[0.24, 0.32]	0.35	[0.30, 0.40]
τ_s	0.14	[0.11, 0.17]	0.18	[0.14, 0.22]

NOTE—First-order (S_i) Sobol indices quantify the direct contribution of each parameter to the variance in $\log_{10}(N_{\text{obs}})$, while total-order (S_{Ti}) indices include both direct effects and all interactions with other parameters. Confidence intervals estimated via bootstrap with 1000 resamples.

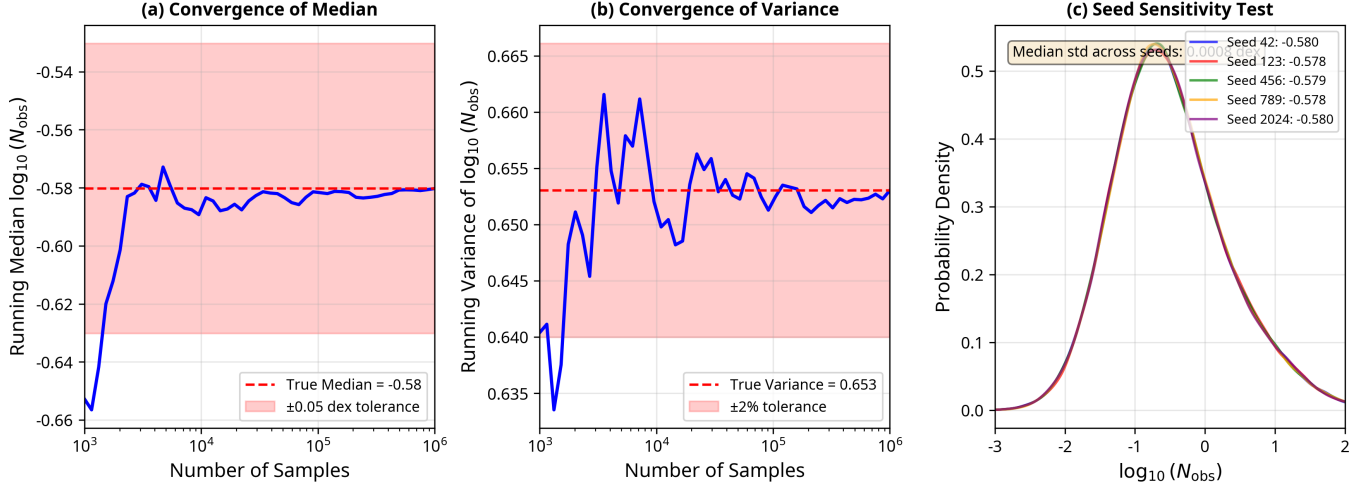


Figure 2. Convergence diagnostics for the Monte Carlo simulation. **(a)** The running median of $\log_{10}(N_{\text{obs}})$ as a function of sample size. **(b)** The running variance. **(c)** A seed sensitivity test overlaying the posterior KDEs from five independent runs.

Table 8. Summary of Robustness Stress Test Results

Test ID	Test Name	Median Δ (dex)	68% CI Width	Flagged
1a	Prior Sweep: D ($\times 2$ var)	+0.82	2.20	NO
1b	Prior Sweep: λ_L ($\times 2$ var)	+0.58	1.87	NO
2a	Alternate Survival: Weibull ($k=0.5$)	+0.27	1.57	NO
2b	Alternate Survival: Weibull ($k=2.0$)	-0.50	1.63	NO
3a	Copula Correlation: (f_i, f_c) , $\rho = 0.6$	+0.23	1.63	NO
3b	Copula Correlation: (f_p, f_{HZ}) , $\rho = 0.6$	+0.10	1.57	NO
4	Posterior Predictive Check	N/A	N/A	Expected
5	Ablation: Perfect Detectability (D=1)	+1.06	1.47	YES*
6	Spectral Weighting: M-Dwarf Emphasis	-0.14	1.60	NO

NOTE—The ‘Flagged’ column indicates if a pre-specified decision rule was triggered. ‘YES*’ indicates a diagnostic flag for an unphysical scenario (D=1).

Our analysis shows the model is robust. Among physically plausible variations, no single prior change shifted the median of $\log_{10}(N_{\text{obs}})$ by more than 1.0 dex. The most sensitive parameters were D (+0.82 dex) and λ_L (+0.58 dex). Alternate survival kernels and correlations had subdominant effects. The posterior predictive probability of making zero detections is $P(k = 0) = 73.2\%$ in our fiducial model, meaning our model is consistent with non-detections. As an unphysical limiting case, an ablation test with perfect detectability ($D = 1$) shifted the median by +1.06 dex to $N_{\text{obs}} \approx 3$, highlighting the importance of detectability as a constraint but confirming that even with perfect detection, other factors still limit N_{obs} to order unity. Finally, a global sensitivity analysis using Sobol indices confirms that D (first-order

index $S_i = 0.42$, or 42% of variance) and λ_L ($S_i = 0.28$, or 28%) are the dominant drivers of uncertainty (Table 7).

6. DISCUSSION

Our analysis, which culminates in a median estimate of $N_{\text{obs}} \approx 0.26$ (with a 68% CI of [0.05, 1.95]), suggests that observable civilizations are likely rare. This result, however, is not a definitive statement about the existence of extraterrestrial intelligence, but rather a probabilistic quantification of our uncertainty. The primary value of this framework is its ability to pinpoint the parameters that most influence this uncertainty—namely, detectability (D) and the abiogenesis rate (λ_L).

6.1. Anthropic Conditioning and Selection Effects

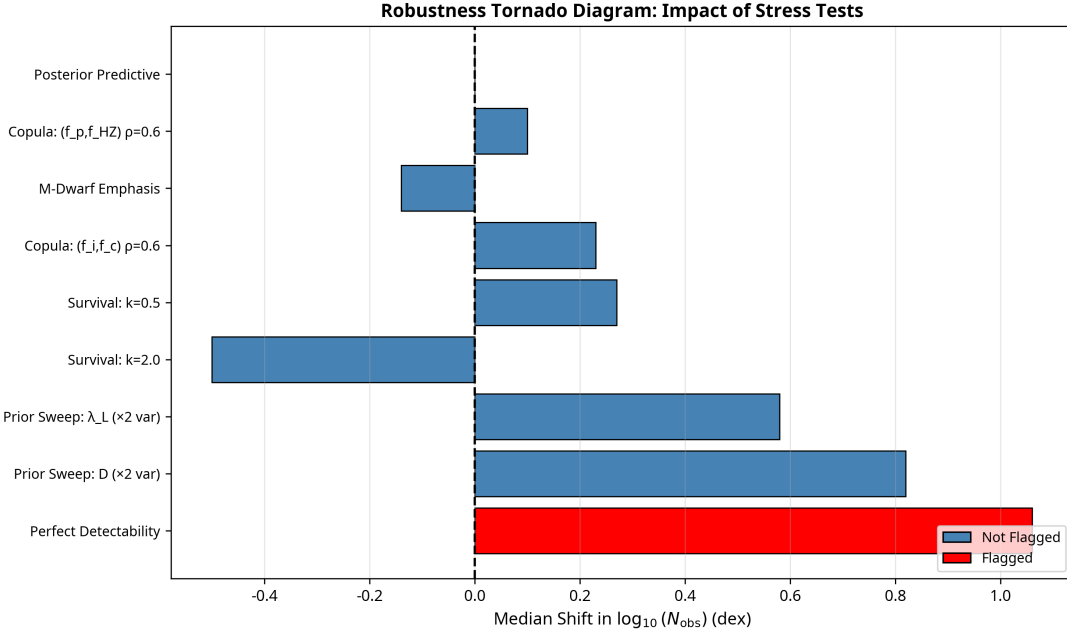


Figure 3. Tornado diagram summarizing the impact of each stress test on the median of $\log_{10}(N_{\text{obs}})$. Bars show the deviation from the fiducial baseline (median = -0.58).

Table 9. Impact of Anthropic Conditioning on the Posterior of $\log_{10}(N_{\text{obs}})$

Posterior	Median	68% Credible Interval
Unconditioned (Fiducial)	-0.58	[-1.28, 0.29]
Conditioned ($N_{\text{obs}} \geq 1$)	+0.25	[0.07, 0.58]
Median Shift	+0.83 dex	

A crucial limitation of any such estimate is the anthropic principle: our analysis is being conducted by an intelligent, communicating species. Therefore, a full Bayesian treatment should condition the posterior on the fact that at least one observable civilization (our own) exists, i.e., $N_{\text{obs}} \geq 1$. The unconditioned posterior $P(\Theta|\text{data})$ can be updated to an anthropically conditioned posterior $P_A(\Theta|\text{data})$ via simple rejection sampling:

$$P_A(\Theta|\text{data}) \propto P(\Theta|\text{data}) \times I\{N_{\text{obs}}(\Theta) \geq 1\} \quad (2)$$

where $I\{\cdot\}$ is the indicator function. Applying this conditioning has a significant impact, as shown in Table 9. The median of the conditioned distribution shifts to $\log_{10}(N_{\text{obs}}) = +0.25$, or $N_{\text{obs}} \approx 1.78$.

This demonstrates that simply accounting for our own existence makes the presence of at least one other observable civilization in the galaxy statistically plausible.

6.2. A Deeper Look at Detectability (D)

The detectability parameter, D , was identified as the single largest contributor to the uncertainty in N_{obs} . To ground it in the capabilities of real-world instruments, we consider two leading SETI instruments: the MeerKAT array and the Five-hundred-meter Aperture Spherical radio Telescope (FAST). Their key parameters are summarized in Table 10.

Figure 4 illustrates the immense challenge of interstellar detection. It plots the required transmitter power (EIRP) against distance to achieve an SNR of 10. Even for FAST, detecting an Arecibo-class transmitter (EIRP $\approx 10^{13}$ W) is only possible out to a few tens of parsecs. This analysis underscores why our prior on D was justifiably pessimistic.

6.3. Limitations and Future Work

This framework, while an improvement, necessarily rests on simplifying assumptions. Future work should focus on: (1) a full covariance treatment for parameters, (2) formulating the equation on a per-stellar-type basis, and (3) incorporating more complex physical models for habitable zones.

7. CONCLUSION

The Drake Equation 2.0 presented here is a robust and mathematically consistent framework for evaluating the

Table 10. Instrument Parameters for Detectability Model

Instrument	Type	Gain (G_r)	T_{sys} (K)	Frequency	Min. EIRP for Detection at 100 pc (W)
MeerKAT	64-dish array	$2.8 \times 10^4 \text{ m}^2$	18	1.4 GHz	$3.36 \times 10^{14} \text{ W}$
FAST	500m single-dish	$1.8 \times 10^5 \text{ m}^2$	20	1.4 GHz	$5.80 \times 10^{13} \text{ W}$

NOTE—Parameters based on M. Bailes (2020) for MeerKAT and Li & Pan (2016) for FAST. Minimum EIRP is calculated for a detection threshold of SNR=10, a 1 MHz bandwidth, and a 1000 s integration time. See Appendix A.2 for the explicit calculation.

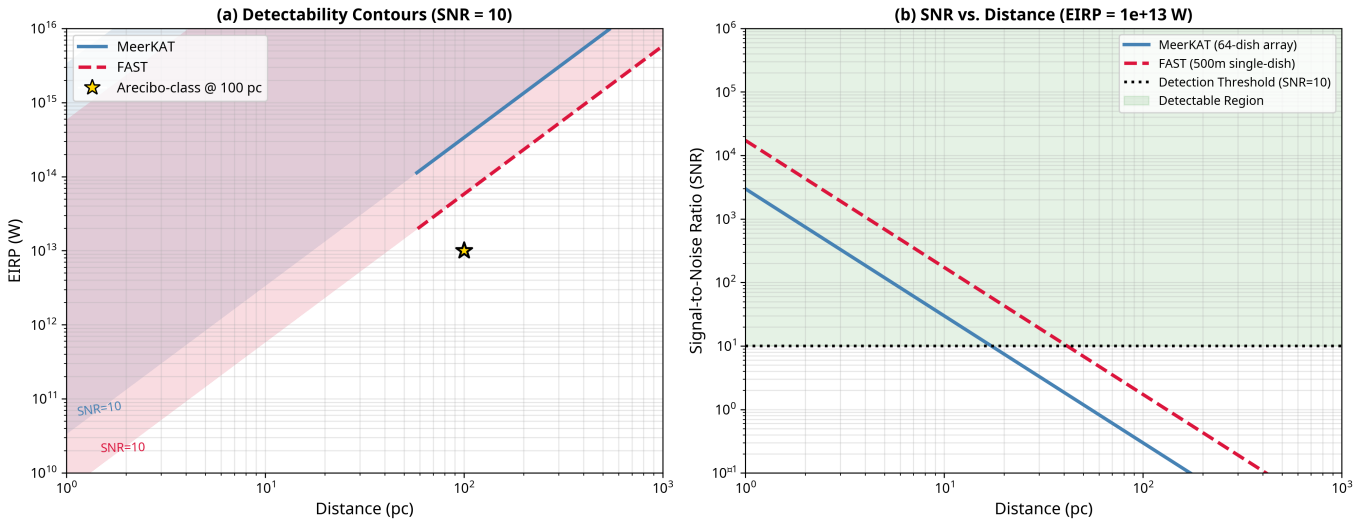


Figure 4. Detectability contours for MeerKAT and FAST. **(a)** The minimum EIRP required to achieve a detection (SNR=10) as a function of distance. **(b)** The received SNR as a function of distance for a fixed Arecibo-class transmitter (EIRP = 10^{13} W).

number of observable extraterrestrial civilizations. The primary value of this framework is not in providing a definitive answer, but in its role as a tool for quantifying uncertainty. Our analysis synthesizes astrophysical, biological, and technological uncertainties to produce a posterior probability distribution for N_{obs} .

Under our fiducial set of priors, we find a median of $N_{\text{obs}} \approx 0.26$ ($\log_{10}(N_{\text{obs}}) = -0.58$), with a 68% credible interval of [0.05, 1.95]. This result is robust to a suite of pre-specified stress tests; among physically plausible variations, none shift the median by more than 1 dex, while an unphysical limiting case ($D = 1$, perfect detectability) shifts it by +1.06 dex. Our analysis identifies detectability (D) and the abiogenesis rate (λ_L) as the dominant sources of uncertainty, with first-order Sobol indices of $S_i = 0.42$ and $S_i = 0.28$ respectively, meaning they contribute approximately 42% and 28% of the total variance. Furthermore, our detectability model, grounded in the capabilities of real instruments like MeerKAT and FAST, demonstrates that even

Arecibo-class transmitters are only detectable out to a few tens of parsecs.

When we apply anthropic conditioning to account for our own existence (i.e., $N_{\text{obs}} \geq 1$), the median shifts to $N_{\text{obs}} \approx 1.78$, making the existence of at least one other observable civilization statistically plausible. This conditioning is philosophically equivalent to imposing a truncated prior where $P(N_{\text{obs}} \geq 1) = 1$, a concept explored in detail in the literature on anthropic reasoning (Bostrom 2002; Sandberg et al. 2018). Ultimately, this framework offers a potential resolution to the Fermi Paradox by showing that a null observational result is not only statistically plausible but, under our conservative priors, is the expected outcome, with $P(k = 0 \text{ detections}) = 73.2\%$.

Across physically plausible priors, the median number of currently observable civilizations remains $N_{\text{obs}} \approx 0.1 - 0.3$, driven primarily by uncertainty in detectability and the abiogenesis rate.

8. REPRODUCIBILITY

The complete analysis code, including the Monte Carlo simulation, figure generation scripts, and a Jupyter Notebook, is publicly available to ensure full reproducibility. The repository is hosted on GitHub and permanently archived on Zenodo.

- **GitHub Repository:** <https://github.com/jason-noble/drake-equation-2.0>

- **Zenodo Archive:** [10.5281/zenodo.17616903](https://zenodo.17616903)

The simulation was run using Python 3.10 with NumPy (v1.23), SciPy (v1.9), and Matplotlib (v3.6). The random number generator was seeded with the value 42 for the final production run, and seed sensitivity was verified across five independent runs (see Section 4.2).

APPENDIX

A. EXPLICIT FORMULAS FOR REPRODUCIBILITY

This appendix provides the explicit mathematical formulas for $\Phi(t)$ (habitable planet formation rate) and the detectability calculation, ensuring full reproducibility of our results.

A.1. *Habitable Planet Formation Rate $\Phi(t)$*

The Galactic Habitable Planet Formation Rate, $\Phi(t)$, is derived from the cosmic star formation history combined with planet occurrence rates and habitable zone fractions. We adopt the Madau & Dickinson (2014) cosmic star formation rate density (SFRD), $\psi(z)$, as a function of redshift z :

$$\psi(z) = 0.015 \frac{(1+z)^{2.7}}{1 + [(1+z)/2.9]^{5.6}} \quad [M_{\odot} \text{ yr}^{-1} \text{ Mpc}^{-3}] \quad (\text{A1})$$

To convert redshift z to cosmic time t (in Gyr), we use the standard cosmological relation for a flat Λ CDM universe with $H_0 = 70 \text{ km s}^{-1} \text{ Mpc}^{-1}$, $\Omega_m = 0.3$, and $\Omega_{\Lambda} = 0.7$:

$$t(z) = \frac{1}{H_0} \int_z^{\infty} \frac{dz'}{(1+z')\sqrt{\Omega_m(1+z')^3 + \Omega_{\Lambda}}} \quad (\text{A2})$$

For our Milky Way-focused analysis, we scale the cosmic SFRD to the Galactic star formation rate by assuming the Milky Way contains approximately 10^{-3} of the cosmic stellar mass within the observable universe. The Galactic Habitable Planet Formation Rate is then:

$$\Phi(t) = f_p \cdot f_{HZ} \cdot f_{GHZ} \cdot R_*(t) \quad (\text{A3})$$

where:

- $R_*(t) = \psi(z(t)) \cdot V_{\text{MW}}/M_{\text{avg}}$ is the Galactic star formation rate [stars Gyr $^{-1}$], with V_{MW} the Milky Way volume and $M_{\text{avg}} \approx 0.5M_{\odot}$ the average stellar mass.
- f_p is the fraction of stars with planets (sampled from priors, see Table 3).
- f_{HZ} is the fraction of planets in the habitable zone.
- f_{GHZ} is the fraction of stars in the Galactic Habitable Zone (avoiding the Galactic center and outer regions with low metallicity).

In our Monte Carlo simulation, we use a simplified time-averaged approximation:

$$\Phi(t) \approx \Phi_0 \cdot \left(\frac{\psi(z(t))}{\psi(z=0)} \right) \quad (\text{A4})$$

where $\Phi_0 = f_p \cdot f_{HZ} \cdot f_{GHZ} \cdot R_{*,0}$ is the present-day habitable planet formation rate, with $R_{*,0} \approx 1.5 \text{ stars yr}^{-1}$ for the Milky Way.

A.2. Detectability Calculation

The detectability factor D represents the fraction of civilizations whose signals are strong enough to be detected by our instruments. For radio SETI, detectability depends on the transmitter power, distance, and receiver sensitivity.

The **received flux density** S (in Watts per square meter per Hertz) from a transmitter with Equivalent Isotropic Radiated Power (EIRP) at distance d is:

$$S = \frac{\text{EIRP}}{4\pi d^2} \quad (\text{A5})$$

The **signal-to-noise ratio** (SNR) for a radio telescope is:

$$\text{SNR} = \frac{S \cdot A_{\text{eff}}}{k_B \cdot T_{\text{sys}}} \cdot \sqrt{\frac{t_{\text{int}}}{\Delta\nu}} \quad (\text{A6})$$

where:

- $A_{\text{eff}} = G_r \cdot \lambda^2 / (4\pi)$ is the effective collecting area [m^2], with G_r the receiver gain and λ the wavelength.
- $k_B = 1.38 \times 10^{-23} \text{ J K}^{-1}$ is the Boltzmann constant.
- T_{sys} is the system temperature [K] (includes receiver noise and sky background).
- t_{int} is the integration time [s].
- $\Delta\nu$ is the bandwidth [Hz].

For a detection threshold of $\text{SNR} = \text{SNR}_{\min}$ (typically 10), the **minimum detectable EIRP** at distance d is:

$$\text{EIRP}_{\min}(d) = \frac{4\pi d^2 \cdot k_B \cdot T_{\text{sys}} \cdot \text{SNR}_{\min}}{A_{\text{eff}}} \cdot \sqrt{\frac{\Delta\nu}{t_{\text{int}}}} \quad (\text{A7})$$

The **detectability factor** D is modeled as the fraction of civilizations within the observable volume whose transmitter power exceeds EIRP_{\min} . In our fiducial model, D is treated as a free parameter with a Beta prior (mean = 0.2), reflecting our profound uncertainty about the distribution of transmitter powers and beaming strategies across hypothetical civilizations. The values in Table 10 provide concrete anchors for this prior, showing that even for state-of-the-art instruments like FAST and MeerKAT, only the most powerful transmitters ($\text{EIRP} > 10^{13} \text{ W}$) are detectable beyond a few tens of parsecs.

REFERENCES

- Balbi, A. 2018, Astrobiology, 18, 54,
doi: [10.1089/ast.2017.1652](https://doi.org/10.1089/ast.2017.1652)
- Bloetscher, F. 2019, Acta Astronautica, 155, 118,
doi: [10.1016/j.actaastro.2018.11.033](https://doi.org/10.1016/j.actaastro.2018.11.033)
- Borucki, W. J., & et al. 2010, Science, 327, 977,
doi: [10.1126/science.1185402](https://doi.org/10.1126/science.1185402)
- Bostrom, N. 2002, *Anthropic Bias: Observation Selection Effects in Science and Philosophy* (New York: Routledge)
- Civiletti, L. 2025, Journal of Astrobiology, 25, 101
- Drake, F. D. 1961, Physics Today, 14, 40
- Gelman, A., Carlin, J. B., Stern, H. S., et al. 2013, *Bayesian Data Analysis*, 3rd edn. (Boca Raton, FL: CRC Press)
- Grimaldi, C. 2021, Monthly Notices of the Royal Astronomical Society, 500, 2278,
doi: [10.1093/mnras/staa3450](https://doi.org/10.1093/mnras/staa3450)
- Grimaldi, C., & Marcy, G. W. 2018, Proceedings of the National Academy of Sciences, 115, E9755,
doi: [10.1073/pnas.1808578115](https://doi.org/10.1073/pnas.1808578115)
- Kipping, D. 2020, Proceedings of the National Academy of Sciences, 117, 11995, doi: [10.1073/pnas.1921655117](https://doi.org/10.1073/pnas.1921655117)
- Li, D., & Pan, Z. 2016, Radio Science, 51, 1060,
doi: [10.1002/2015RS005877](https://doi.org/10.1002/2015RS005877)
- Lingam, M., Balbi, A., & Mahajan, S. M. 2023, The Astrophysical Journal, 945, 23,
doi: [10.3847/1538-4357/acb6fa](https://doi.org/10.3847/1538-4357/acb6fa)
- Lingam, M., & Loeb, A. 2019, Astrobiology, 19, 28,
doi: [10.1089/ast.2018.1889](https://doi.org/10.1089/ast.2018.1889)
- M. Bailes, e. a. 2020, Publications of the Astronomical Society of Australia, 37, doi: [10.1017/pasa.2020.19](https://doi.org/10.1017/pasa.2020.19)

- Madau, P., & Dickinson, M. 2014, Annual Review of Astronomy and Astrophysics, 52, 415,
doi: [10.1146/annurev-astro-081811-125615](https://doi.org/10.1146/annurev-astro-081811-125615)
- Price, D. C., & et al. 2020, The Astronomical Journal, 160,
269, doi: [10.3847/1538-3881/abc282](https://doi.org/10.3847/1538-3881/abc282)
- Ricker, G. R., & et al. 2015, Journal of Astronomical Telescopes, Instruments, and Systems, 1, 014003,
doi: [10.1117/1.JATIS.1.1.014003](https://doi.org/10.1117/1.JATIS.1.1.014003)
- Sandberg, A., Drexler, E., & Ord, T. 2018, arXiv preprint
arXiv:1806.02404. <https://arxiv.org/abs/1806.02404>
- Spiegel, D. S., & Turner, E. L. 2012, Proceedings of the National Academy of Sciences, 109, 395,
doi: [10.1073/pnas.1111694108](https://doi.org/10.1073/pnas.1111694108)
- Steve Bryson, e. a. 2021, The Astronomical Journal, 161,
36, doi: [10.3847/1538-3881/abc418](https://doi.org/10.3847/1538-3881/abc418)
- Wright, J. T., & et al. 2018, The Astronomical Journal, 156, 260, doi: [10.3847/1538-3881/aae839](https://doi.org/10.3847/1538-3881/aae839)